A Frequency Domain Stability Analysis of a Phase Plane Control System

Alexander N. Penchuk* and Philip D. Hattis†
The Charles Stark Draper Laboratory, Cambridge, Massachusetts

and

Edward T. Kubiak‡
NASA Johnson Space Center, Houston, Texas

A describing function is used to model a phase plane controller which is part of the Space Shuttle on-orbit Reaction Control System autopilot. A frequency domain stability analysis of the closed-loop control system is applied to a study of potential flight control system interaction with the Orbiter and a class of payloads deployed from a tilt table. Phase-gain plot techniques are used to show that expansion of phase plane angular rate limits and stiffening of the tilt table pivot do not always enhance system stability. Instability region approximations are mapped as a function of rate limit, payload geometry, jets used, and natural frequency of the pivot. Comparison of the describing function analysis with simulation results shows excellent correlation.

Nomenclature

$\bar{F}_i$ = planar force due to jet firing
$G(s)$ = composite forward loop linear transfer function
G_B = bending dynamics transfer function
G_R = rigid-body dynamics transfer function
G_{SE} = approximate state estimator transfer function
i = index ranging from 1 to 2
I_{ORB} = Orbiter planar moment of inertia about its center of mass
I_{PL} = payload planar moment of inertia about its center of mass
IUS = Inertial Upper Stage
$M_{CB,i}$ = torque about the composite body center of mass due to $\bar{F}_i$
m_{ORB} = Orbiter mass
m_{PL} = payload mass
$N(\alpha)$ = nondimensional nonlinearity representing the phase plane switching logic
$\bar{r}_1$ = planar vector from Orbiter center of mass to pivot
$\bar{r}_2$ = planar vector from pivot to payload center of mass
RL = angular rate limit from phase plane
s = frequency domain variable from Laplace transform
T = IMU sensor read delay time
α = nondimensional input amplitude to N
β = nondimensional payload specific geometry/mass/force parameter
γ = parameter representing available Reaction Control System control acceleration
ζ_e = state estimator damping ratio using second-order model
ζ_p = natural damping ratio of the payload/Orbiter system (0.5%)
ω = model input oscillation frequency
ω_e = state estimator break frequency using second-order model
ω_p = pivot bending natural frequency

Received July 19, 1983; revision received Dec. 1, 1983.

*Technical Staff. Member AIAA.
†Technical Staff. Member AIAA.
‡Engineer.
Editor's Note: We regret to note that Mr. Penchuk died on Feb. 22, 1983.

Introduction

MANY space vehicles employ "on/off" thrusters as control effectors. The design of control systems with these elements frequently use a phase plane to define regions for switching thrusters "on" or "off" depending on the state of the system. For second-order systems, the phase plane trajectories are analytical and the system behavior can be readily predicted.[1] However, the phase plane control laws are nonlinear and an increase in complexity of the system due to the introduction of sensor data delays, filters, flexural dynamics, quantization, noise, and sampling rates makes behavioral analysis considerably more difficult, generally causing computer simulation to be substituted for mathematical analysis.

Replacement of the phase plane controller with an approximate analytic model which considers angular rate errors while neglecting the effect of attitude errors enables application of describing function analysis for characterization of system stability boundaries. Gain and phase margins can be estimated, and the effect of the phase plane rate limit variations on system stability can be evaluated.

The Space Shuttle on-orbit flight control system was modeled using the describing function method. The analytical tool then was combined with a simple Orbiter/payload dynamical model to permit studies of the interaction of the Shuttle Orbiter with payloads which pivot on a tilt table during deployment.

Many large Shuttle payloads are deployed by means of a tilt table with a pivot near the aft end. After the payload is tilted upward, it is launched with springs (Fig. 1).[2] Dynamic interaction of Orbiter and payload due to flexure at the pivot is a major concern. Such problems have been studied in the past using high-fidelity simulations which are payload specific,[3,4] costly, and provide little insight into the general problem. This

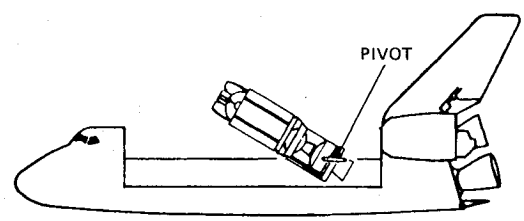

Fig. 1 Tilt table deployment of IUS and satellite.

paper demonstrates that the describing function techniques can be used successfully to model the Shuttle phase plane characteristics, which in turn permit stability predictions of an Orbiter/payload system connected by a tilt table. The results are shown to be consistent with simulation.

Problem Statement

Consider a standard control loop (Fig. 2). The behavior of this system can be studied analytically with classical frequency domain techniques if one can write frequency domain equations for each of the elements.

To do an analytical study of the Shuttle/payload control loop it is necessary to fit the system dynamics into a model similar to Fig. 2. The spacecraft on-orbit Reaction Control System (RCS) autopilot contains three basic elements: a per-axis phase plane algorithm, jet selection logic, and a rotation state estimator which only uses Inertial Measurement Unit (IMU) attitude data and feed-forward prediction from the jet selection.[5,6] The first two elements comprise the controller. The controller operates effectors including 38 870-lbf primary thrusters and 6 24-lbf vernier thrusters at various forward and aft locations on the Orbiter. The standard plant represents the dynamical response of the Orbiter/payload system to the effectors. Finally, the state estimator provides the feedback to close the control loop.

The controller transfer function is nonlinear due to the complex switching logic of the phase plane as shown in Fig. 3. The phase plane often has been perceived as an idealized method of treating performance optimization for classes of minimum time and/or minimum fuel problems[1] although in most practical applications many modifications to the ideal switch line logic are required. In the Orbiter autopilot application, attitude control is considered on a per-rotation-axis (planar motion) basis with a phase plane constructed from an estimated attitude error on the horizontal axis and an estimated angular rate error on the vertical axis. Jet command switch lines are determined by limits on acceptable state error magnitudes. The parabolic switchlines near the deadband are shaped by preflight estimates of RCS acceleration in the particular axis. A "shelf" with a width equal to 20% of the deadband is added on the attitude axis to capture shallow or "delayed" phase plane trajectories back within the central switch region. Shallow trajectories may result from cross-axis coupling or a disturbance torque (e.g., venting). "Delayed" or shifted trajectories can result from sampling or transport delays which forestall the corrective thruster firing until the state is slightly past the switching line. Between the parabolic switch lines, hysteresis is applied to quickly reduce transient rates in excess of angular rate limits and to minimize jet chatter. Within the hysteretic region the "off" command switch-line is biased by a disturbance acceleration measure from the state estimator in order to prevent chattering on deadband switchlines induced by disturbance torques. The anticipated disturbance levels are very small ($< 10^{-4}$ deg/s^2) and often are tied to partial orbit periodicity which leads to a long acceleration estimate rise time ($\sim$ 56 s). The spectrum of interaction frequencies of interest is well above the acceleration estimate bandwidth making the biasing effect negligible. As a result it is not included in the simplified phase plane switching model discussed later. Large attitude errors are efficiently reduced by trapping the phase plane trajectory in a drift channel at a rate near the rate limit. Also, expected coupling between rotation axes is explicitly considered during vernier jet operations by producing fractional command preferences on the basis of phase plane position within the hysteretic region or drift channels. A more complete discussion of the switching logic is in Ref. 7.

The state estimator derives attitude, rate, and acceleration estimates; however, as discussed earlier, the acceleration estimate is not important in the problem under consideration. Whereas the attitude estimate is nearly a direct pass use of the attitude measurement, the rate estimate is a combination of jet selection feed-forward prediction (open-loop calculation of expected rigid-body, thruster-induced, rate changes) and an

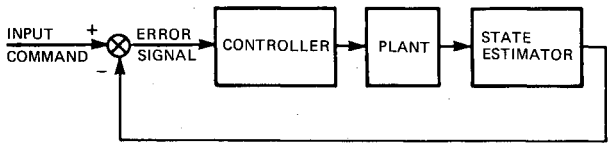

Fig. 2 Standard control loop.

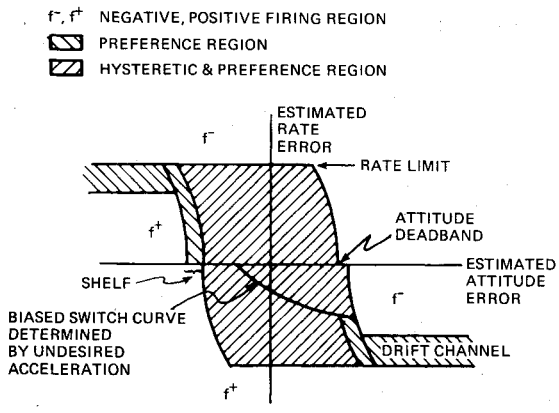

Fig. 3 On-orbit rotation control phase plane switch lines and regions for a single rotation axis.

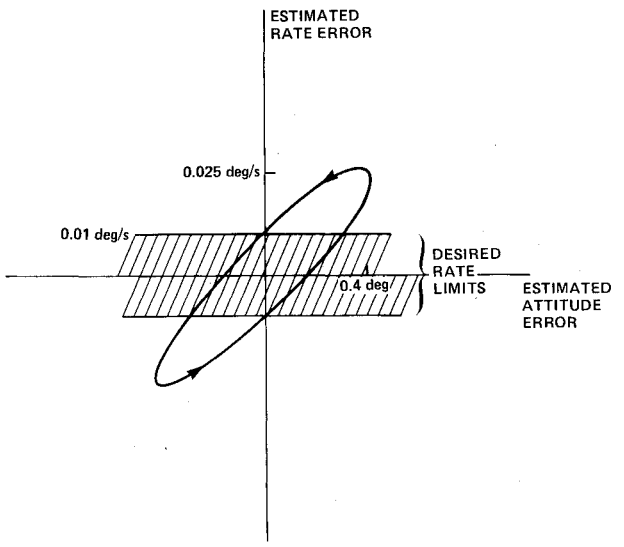

Fig. 4 Estimated state phase plane trajectory for a rate oscillation of amplitude greater than the rate limit.

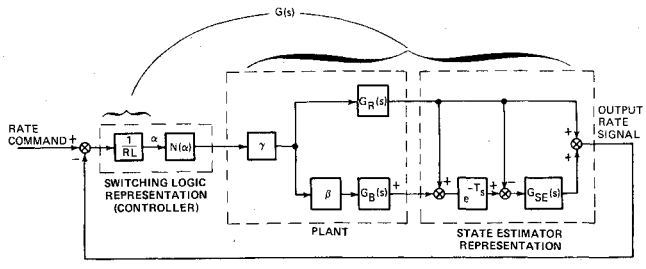

Fig. 5 Planar rate control loop model in the frequency domain.

approximately second-order attitude filter, the characteristics of which are given later, which corrects the feed-forward extrapolation rate. The feed forward reduces peak errors due to filter lag while the filter portion nulls errors due to sample delay, feed-forward inaccuracy, and rate changes from sources other than thruster firings.

The payload/Orbiter dynamics can be represented linearly as two rigid bodies connected by a torsion spring at the pivot. Other Orbiter frequencies, or tilt table class payload frequencies, will be well above the angular rate estimator bandwidth (~ 0.04 Hz for vernier jets).

For the range of frequencies typically experienced at the pivot with tilt table deployed payloads, it is far more likely that a system vibrationally excited by the RCS activity which initially is in response to rigid-body control requirements will periodically exceed angular rate limits before it is excited enough to cause forced attitude deadband oscillations. Figure 4 shows a typical limit cycle for a payload discussed in Ref. 4 which is initially excited by RCS activity under tight vernier control. The rate limit selected was 0.01 deg/s, while the deadband was around 1 deg. A sustained rate oscillation was easily achieved. The counterclockwise phase plane trajectory is a consequence of the plot being against the estimated errors which determine the autopilot control actions. Lags due to state estimator frequency response, phase plane deadzone effects, and transport delay add up to cause phase plane commands to be issued at times quite different than would be desired if perfect state knowledge were available. The net result is to demonstrate that with typical angular rate limit and attitude deadband combinations, an oscillation easily can be sustained that does not interact with the deadband. Limit cycles in other phase plane regions need not be considered since data source biases affecting the phase plane axes realistically cannot be large enough to be significant. This suggests the simplification of modeling the phase plane as only a rate control nonlinearity. Further discussion of limit cycles with the Shuttle on-orbit autopilot is in Ref. 4.

A detailed version of Fig. 2 including the phase plane simplification, the Orbiter/payload dynamics, and the state estimator implementation is shown in Fig. 5. $N(\alpha)$ is a nondimensionalized rate control nonlinearity illustrated in the middle of Fig. 6 which replaces the phase plane and has an input error signal α. The phase plane rate limit (RL) is used to nondimensionalize the nonlinearity input. The parameter γ is equivalent to the RCS control authority with acceleration dimensions, and is used to nondimensionalize the nonlinearity output resulting from commanded jet firings. The dimensionless parameter β is an Orbiter/payload/RCS jet configuration dependent parameter which is strongly influenced by the payload effect on the composite system rotational inertia and the force/torque characteristic of crew-selected thrusters. It is discussed more later and derived in detail in Ref. 8. G_R is the rigid-body transfer function representing the feed-forward extrapolation of rates from the jet selection. G_B is the bending dynamics of the payload/Orbiter system modeled as a complex quadratic pole with ω_p defined to be the free payload frequency when attached to the Orbiter and ζ_p assumed to be 0.5% structural damping. The relation of the ground test pivot frequency and ω_p is explained later. T is the delay time in the IMU sensor processing. G_{SE} is the second-order filter representation of the state estimator which only affects the signal not fed directly forward. Since the rigid-body motion is sensed by the IMU and is passed along with a sensor delay, a residual after the delay goes to the state estimator along with bending dynamics.

The transfer functions, time delay, and estimator coefficients are given in Table 1.

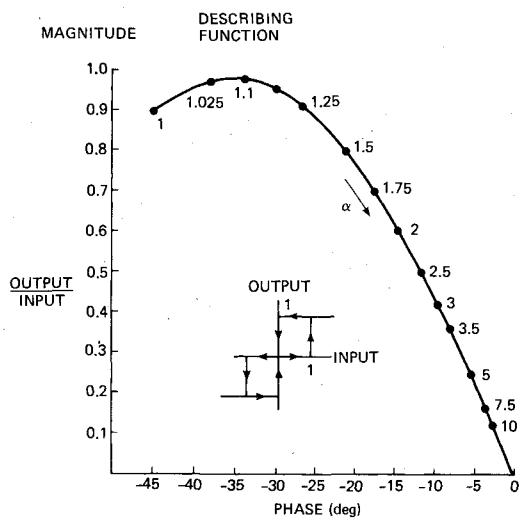

Fig. 6 Describing function gain and phase properties.

Table 1 System model transfer functions

Dynamical element	Value
$G_B(s)$	$s/(s^2 + 2\zeta_p\omega_p s + \omega_p^2)$
$G_R(s)$	$1/s$
$G_{SE}(s)$	$\omega_e^2/(s^2 + 2\zeta_e\omega_e s + \omega_e^2)$
$N(\alpha)$	$\frac{2}{\pi\alpha^2}\left(\alpha + \sqrt{\alpha^2 - 1} - j\right)$ for $\alpha \geq 1$
	0 for $\alpha < 1$
T	0.312 s
ζ_e (for vernier jets)	0.5
ω_e (for vernier jets)	0.2513 rad/s

Frequency Domain Analysis

Having decided to be concerned primarily with angular rate oscillations, it is necessary to find a frequency domain equivalent for $N(\alpha)$. The phase plane control degenerates to a hysteretic rate relay as the attitude deadbands get very large. The "on" threshold for jets is at the rate limit. The "off" threshold is assumed at zero rate which neglects the disturbance acceleration effects for the reasons already discussed. Sinusoidal input describing functions permit simple approximate frequency domain representations of relay-like nonlinearities.[9] Figure 6 plots the nonlinearity's describing function frequency domain properties with the input assumed to be of the form $\alpha\sin\omega t$.

The methodology for evaluating the stability of the control system model involves well-known phase-gain plot techniques. For strictly linear systems, stability can be discerned from the relative position of the point at -180-deg phase and unity magnitude to the plot of the open-loop transfer function.

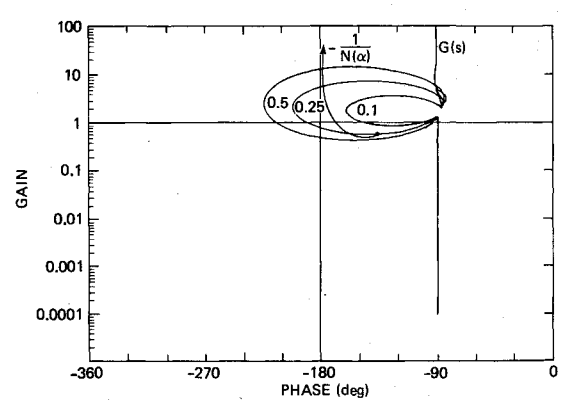

Fig. 7 Phase-gain characteristics for (RL/γ) = 0.5 s, ω_p = 0.1 Hz, β varied (0.1, 0.25, 0.5).

When there is a forward-loop nonlinearity, stability is assessed approximately on the basis of the proximity of the plot of the product of the nonlinearity representation and the linear transfer function to the same point at -180-deg phase. Alternately, the existence of intersections between the linear function and the negative reciprocal of the nonlinearity describing function in the phase-gain space can be used to assess stability. Since many system properties are illustrated better by separately plotting the linear and nonlinear components, that technique is the method of choice.

With a nonlinear system, phase-gain plot intersections can sometimes mean that stable limit cycles exist without external excitation. While the resultant amplitude of oscillation is bounded, these limit cycles are unstable for our purposes since they result in an unconstrained RCS propellant consumption even when disturbances are eliminated.

Properties of the Phase-Gain Plots

The phase-gain plot analysis must be characterized with a few examples to permit later interpretation of stability boundary sensitivities.

Figure 7 plots the nonlinearity against three transfer functions with different values of β and constant pivot frequency. The other parameters assigned apply to tight rate control with vernier jets. Sufficiently low values of β assure no intersection, making instabilities unlikely. Larger values of β can result in one, two, or possibly three intersections depending on how the nonlinearity plot "fishhook" is approached.

Figure 8 plots the nonlinearity against three transfer functions with different pivot bending frequencies and constant β. Tight vernier rate control is again considered. No intersections are apparent between the nonlinearity and the linear transfer functions, implying that all are likely to be stable. Phase and gain stability margins may be approximated by the relative approach distance of the different linear plots to the describing function plot. Stiffer pivots with higher frequencies result in smaller linear plot loops which eventually move down and away from possible nonlinearity plot intersections. However, because of the "fishhook," a slight increase in pivot stiffness can sometimes decrease stability margins and may induce instability with unusual combinations of parameters.

Rate limit increases proportionately move the loop of $G(s)$ down relative to the nonlinearity plot, which eventually would eliminate any chance of intersections. It is evident in both Figs. 7 and 8, however, that the "fishhook" will intersect some plotted linear transfer function curves with rate limit increases of less than a factor of 10, greatly increasing the chances of instability.

The phase-gain plots not only help determine system stability, but clearly illustrate the nonintuitive result that increasing the pivot stiffness or the phase plane angular rate control deadzone limit do not improve system stability margins automatically.

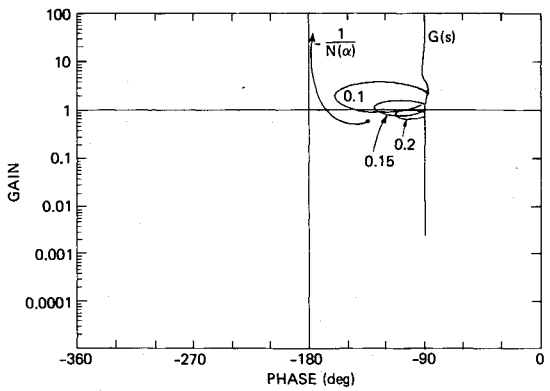

Fig. 8 Phase-gain characteristics for $(RL/\gamma) = 0.5$ s, $\beta = 0.1$, ω_p varied (0.1, 0.15, 0.2 Hz).

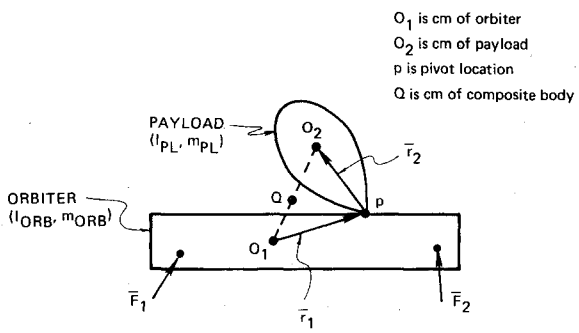

Fig. 9 Two-body system connected by a pivot spring.

Evaluating β

The details of the Shuttle payload parameter reduction to develop the nondimensional quantity β are provided elsewhere,[8] but Fig. 9 and Table 2 are provided as a summary. The computation of γ and the relationship between ω_p and the constrained ground test frequency are also given. (In practical application, the different pivot frequency representations have almost the same value.)

Since we are interested in steady-state stability, it is assumed that the net angular momentum change over one flexural cycle is zero with opposing jet firing rotation impulses over one jet firing cycle equal in magnitude. Furthermore, it is assumed that the signal driving the Orbiter and payload equations of motion can be approximated by a symmetric single frequency sinusoid. (This is consistent with an assumption implicit in the describing function derivation.) This is accomplished by requiring that the fundamental frequency term of the Fourier series of the approximate signal equal the fundamental frequency term of the actual signal, with higher harmonics neglected. Unfortunately, the "gain" β in the bending loop which results from this approach can depend on the duty cycle, i.e., the proportion of jet "on" time. For the Shuttle, opposing roll and yaw firings produce nearly symmetric torques. However, for pitch the control authority is very different in the two directions due to RCS cluster positions and impingement of some jet plumes on Orbiter structure. If opposing jets are on for equal lengths of time (as for roll and yaw), then β is independent of the duty cycle. In pitch, where

Table 2 Formulas to compute payload dependent parameters

Intermediate variables

$$\mu = \frac{m_{PL} m_{ORB}}{m_{PL} + m_{ORB}} \qquad \Delta M_{CB} = M_{CB,1} - M_{CB,2}$$

$$\alpha_{11} = I_{ORB} + I_{PL} + \mu|\bar{r}_1 + \bar{r}_2|^2 \qquad M_0 = \frac{-2M_{CB,1}M_{CB,2}}{\Delta M_{CB}}$$

$$\alpha_{12} = I_{PL} + \mu \bar{r}_2 \cdot (\bar{r}_1 + \bar{r}_2) \qquad k = M_{CB,1}/M_{CB,2}$$

$$\alpha_{22} = I_{PL} + \mu|\bar{r}_2|^2 \qquad F_{2,i} = -\bar{r}_2 \times \bar{F}_i$$

$$D = \alpha_{11}\alpha_{22} - \alpha_{12}^2 \qquad A_i = M_{CB,i} - \frac{\mu\alpha_{11}}{m_{ORB}\alpha_{12}} F_{2,i}$$

$$A_0(\zeta) = \frac{A_1 \sin\zeta - A_2 \sin k\zeta}{2\sin\left(\frac{1+k}{2}\zeta\right)} \quad \text{for } 0 \le \zeta \le \frac{\pi}{1+k}$$

$A_0^* = \max[A_0(\zeta)]$ if $A_0 > 0$
$= \min[A_0(\zeta)]$ if $A_0 < 0$
consider both if A_0 ranges from positive to negative

Resultant parameters

$$\beta = A_0^* \alpha_{12}^2 / M_0 D, \qquad \gamma = M_0/\alpha_{11}$$

$$\omega_p = \omega_{\text{constrained}} \left[\frac{\alpha_{11}}{D}\left(I_{PL} + m_{PL}|\bar{r}_2|^2\right)\right]^{\frac{1}{2}}$$

the opposing jet "on" times are unequal, a conservative approach is to calculate the extreme values of β for a particular payload and set of jets. This would be based on duty cycles ranging from the low value of the direction with greatest control authority to the high value of the direction with least control authority. Use of the extreme β values to check against the results of the stability analysis of the simplified system can help predict if instability is possible.

In some situations there is a clear physical interpretation for β. If the payload rotation in response to Orbiter jet translation forces is opposite in sign and greater in magnitude than the response to Orbiter jet rotation torques, then β is negative. Otherwise, β is positive. Also, in the degenerate planar case where the pivot, payload center of gravity, and Orbiter center of gravity are coincident, then β reduces to the ratio I_{PL}/I_{ORB}.

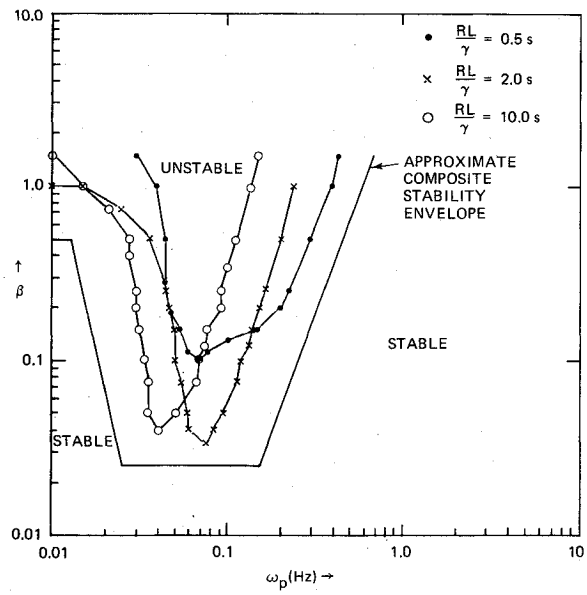

Fig. 10 Some stability boundaries for the vernier jets with $\beta > 0$ (boundaries imply zero margin).

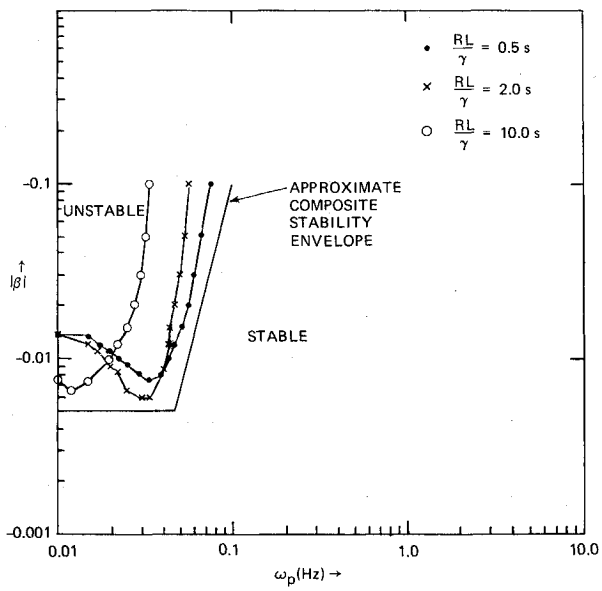

Fig. 11 Some stability boundaries for the vernier jets with $\beta < 0$ (boundaries imply zero margin).

Some Results of Stability Analysis

Phase-gain plots of the type shown in Figs. 7 and 8 can be generated for parametric variations in the pivot frequency, the payload dependent parameter β, and the required rate control precision. The results can be used to plot regions of instability as shown in Fig. 10 which depicts results for the vernier jet operation with positive β. Each of the three curves reflect the approximate stability boundary as a function of β and ω_p for different rate control precisions. If $\gamma = 0.02$ deg/s^2, a typical upper limit for vernier accelerations on the Shuttle, then the curves represent separate stability boundaries for rate limits of 0.01, 0.04, and 0.20 deg/s.

Figure 10 illustrates that the intuitive conclusion that an increase in rate limit, which increases the required amplitude to sustain an oscillation, should enhance stability is partly correct. The right side of the instability boundary moves to lower frequencies for larger rate limits. However, an increase in rate limit can, under some circumstances, reduce the lowest value of β where instability exists.

The left boundary of the instability regions in Fig. 10 also moves to lower frequencies for rate limit increases which imply that some payloads with low frequencies at the pivot can be destabilized by increasing rate limits, a point that may not have been obvious without the describing function analysis. This effect is the result of the way the linear transfer function phase-gain plot loops move relative to the nonlinearity "fishhook" as the pivot frequency and rate limits are varied. Physically this may be understood in situations where the duty cycle is sufficiently high that there is a direct relation between flexure cycle period and the duration of each jet "on" command. Under the stated conditions, larger rate limits, which cause longer jet firings, lead to lower frequency excitation.

An envelope can be drawn around all the approximate instability boundaries for a wide range of rate limits. For the payload designer with control of pivot stiffness or β value it would seem prudent to avoid the entire instability envelope by a considerable margin.

Figure 11 plots the approximate stability boundaries for the same RL/γ values as in Fig. 10 but for negative β. Once again, the right boundary is pushed left when rate limits are increased for fixed γ with the effect of expanding the high-frequency stability region. However, as with positive β, some

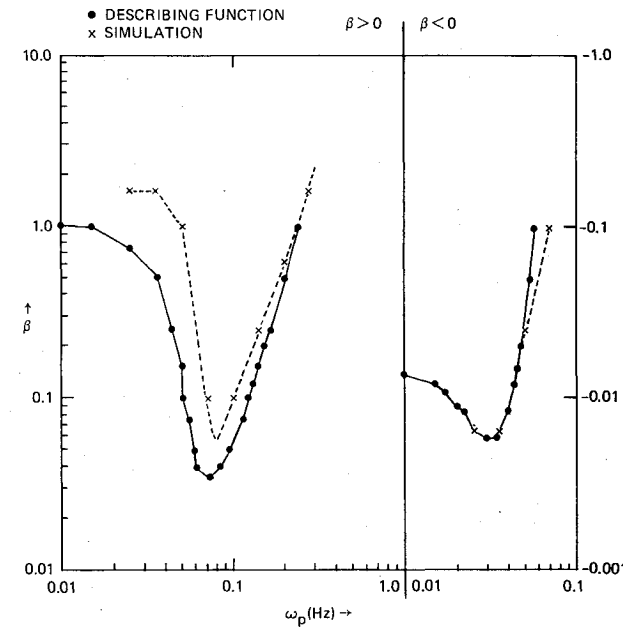

Fig. 12 Comparison of describing function analysis and simulation for RL/γ = 2 s.

payloads with relatively low pivot frequency may be destabilized by increasing rate limits due to the dips in each of the boundaries which move left with increasing rate limit. Again, an envelope can be drawn to define a high confidence stability boundary for a wide range of rate limits.

Figure 12 plots the stability boundaries for a single RL/γ value derived by the describing function technique along with some simulation points from work done for Ref. 8. (The figure is split to show both positive and negative β.) For positive β, the trends are similar, the right boundary is very close, and the left boundary is somewhat more conservative for the describing function results. For negative β, the agreement is almost perfect.

In general, it has been found that the parameter sensitivity trends are similarly predicted by simulations and the describing function analysis. However, the stability boundaries are consistently slightly more conservative with the describing function approach. This may be both because the describing function analysis is an approximation and because it draws stability conclusions on the basis of whether any intersections exist in the phase-gain diagram regardless of how unlikely it may be to inadvertently induce the sequence of RCS inputs required to cause a sustained forced oscillation larger than the phase plane rate limits. Observation of instability via simulation requires that inputs capable of destabilizing the system somehow be duplicated.

Conclusions

The Shuttle Orbiter during payload operations, a complex dynamical system/control system loop including a nonlinear phase plane control law and "on/off" effectors, has been successfully studied in the frequency domain through the use of a describing function model of the nonlinearity with associated approximations. In application of the technique to stability analysis of the on-orbit Reaction Control System during deployment of a class of payloads using tilt tables, good agreement was shown between the describing function results and simulation.

The analytical treatment allows general statements to be made about system stability characteristics which will help payload designers and Shuttle mission planners. Approximate stability regions can be defined as a function of tilt table pivot frequency, payload design parameters, which jets are used, and phase plane parameters. Results suggest that for high tilt table pivot stiffnesses, an increase in angular rate limit is likely to increase stability margin. However, for some payloads with relatively low pivot frequencies, rate limit increases may destabilize the payload/Orbiter configuration. In all situations, phase and gain margins can be estimated, and instability predicted with reasonable confidence without resort to detailed high-fidelity simulations.

Acknowledgments

This paper was partly prepared by The Charles Stark Draper Laboratory, Inc., under Contract NAS-9-16023 with NASA. The work was supported by NASA Johnson Space Center. Publication of this report does not constitute approval by NASA of findings or conclusions contained herein. It is published for the exchange and stimulation of ideas.

References

[1]Athans, M. and Falb, P.L., *Optimal Control*, McGraw-Hill Book Co., New York, 1966, pp. 504-749.

[2]"Flight Data File Payload Deploy Checklist, STS-6, IUS/TDRS-A," NASA JSC 18181 Final, Revision A, Jan. 5, 1983.

[3]"Space Shuttle On-Orbit Flight Control System/IUS Payload Dynamics Interaction Study," Report CSDL-R-1445, Charles Stark Draper Lab., Cambridge, Mass., Feb. 1981.

[4]Sackett, L.L. and Kirchwey, C.B., "Dynamic Interaction of the Shuttle On-Orbit Flight Control System with Deployed Flexible Payloads," *Proceedings of the AIAA Guidance and Control Conference*, San Diego, Calif., Aug. 1982, pp. 232-245.

[5]Nakano, M.M. and Willms, R.L., "Space Shuttle On-Orbit Flight Control System," *Proceedings of the AIAA Guidance and Control Conference*, San Diego, Calif., Aug. 1982, pp. 429-436.

[6]Hattis, P.D., "Qualitative Difference between On-Orbit and Transition RCS Control," *Proceedings of the AIAA Guidance and Control Conference*, San Diego, Calif., Aug. 1982, pp. 437-442.

[7]Hattis, P. et al., "Shuttle On-Orbit Flight Control Characterization (Simplified Digital Autopilot Model)," NASA JSC 18511, Aug. 1982.

[8]Kirchwey, C.B. and Sackett, L.L., "Stability of the Shuttle On-Orbit Flight Control System for a Class of Flexible Payloads," *Proceedings of the AIAA Guidance and Control Conference*, Gatlinburg, Tenn., Aug. 1983, pp. 128-141.

[9]Gelb, A. and Vander Velde, W.E., *Multiple Input Describing Functions and Nonlinear System Design*, McGraw-Hill Book Co., New York, 1968.